Colloids and Surfaces B: Biointerfaces 181 (2019) 1004–1011

Contents lists available at ScienceDirect

Colloids and Surfaces B: Biointerfaces

journal homepage: www.elsevier.com/locate/colsurfb

Using chemical bath deposition to create nanosheet-like CuO electrodes for supercapacitor applications

S.K. Shinde[a], H.M. Yadav[b], G.S. Ghodake[a], A.A. Kadam[c], V.S. Kumbhar[d], Jiwook Yang[a], Kyojung Hwang[a], A.D. Jagadale[e], Sunil Kumar[f], D.Y. Kim[a,*]

[a] Department of Biological and Environmental Science, College of Life Science and Biotechnology, Dongguk University, 32 Dongguk-ro, Biomedical Campus, Ilsandong-gu, Siksa-dong, 10326 Goyang-si, Gyenggi-do, South Korea
[b] Department of Energy and Materials Engineering Dongguk University Seoul, 04620, South Korea
[c] Research Institute of Biotechnology and Medical Converged Science, Dongguk University, Biomedi Campus, Ilsandong-gu, Goyang-si, Gyeonggi-do, 10326, South Korea
[d] School of Nano & Materials Science and Engineering, Department of Energy Chemical Engineering, Kyungpook National University, 2559, Gyeongsang-daero, Sangju, Gyeongbuk, South Korea
[e] Department of Electrical Department of Electrical and Computer Engineering, Kettering University, Flint, MI, 48504, USA
[f] Nano Information Technology Academy, Dongguk University, Seoul 100715, South Korea

ARTICLE INFO

Keywords:
Chemical synthesis
Nanosheets
Supercapacitor
Specific capacitance
Ionic liquid

ABSTRACT

We report the effect of ionic liquids on chemically synthesized hierarchical-like copper oxide (CuO) thin films for supercapacitor applications. Concisely, the CuO thin films were deposited via chemical bath deposition (CBD) using 2-dimethylimidazolium chloride [HPDMIM(C1)], 1-(2′,3′-dihydroxypropyl)-3-methylimidazolium chloride [DHPMIM(C1)], and *N*-(3-methyl-2-oxopropyl)pyridine chloride [MOCPP(C1)] ionic liquid solvents. The effects of the ionic liquid solvents on the morphological evolution of the as-prepared films were analyzed, and electrochemical properties were investigated. The highest specific capacitance was achieved for the electrode with a nanosheet-like structure produced by functionalization with the HPDMIM(C1) ionic liquid. The maximum specific capacitance achieved for the HPDMIM(C1):CuO hybrid electrode was 464 F g^{-1} at 5 mV s^{-1} in a 1 M Na_2SO_4 electrolyte. Thus, our findings, in addition to the stability of the HPDMIM(C1):CuO, indicate that it is a candidate for energy-storage applications.

1. Introduction

Increasing worldwide energy demand has played a catalytic role in the advancement of several energy storage technologies [1]. Two of the most important factors in energy storage research is renewability and sustainability [1–4]. Many researchers are currently focusing on addressing problems regarding energy storage technologies such as batteries and supercapacitors [4–9]. The main motivation in the case of supercapacitors is to improve their performance because these devices can supply very high power compared with batteries and other electronic devices [1–6]. Supercapacitors are distributed into three core types: electrochemical-double-layer capacitors, pseudocapacitors, and hybrid capacitors [1,5–9]. All three supercapacitor types have high charge–discharge rates, high power densities, long lifecycles, and safe operating processes [2,2,3,4].

Copper oxides are useful in various applications involving heterogeneous catalysis [5–9], gas sensing [10], photoelectrochemical cells [11], and supercapacitors [12]. They have been extensively investigated as an electrochemical material for supercapacitors because of their high abundance in the earth's crust, low cost, low toxicity, and good charge transport properties, all of which are beneficial in supercapacitor applications. The copper oxide are two common phases likes copper (II) oxide (CuO) and copper (I) oxide (Cu_2O) [13–15]. Different CuO nanostructures have been prepared and applied in supercapacitors, including flower [16,17] and nanoflakes [18], willow-leaves [19], micro-roses and micro-wool [20], nanosheets [21,22], nanospheres [23], nanoplatelets [24], nanowires [25], nanoribbons and nanoflowers [26], dandelion-like CuO microspheres [27], and nanorods [28].

Several methods have been used to prepare CuO and Cu_2O electrodes for supercapacitors [29–35]. Ghasemi et al. [36] reported using electrodeposited Cu_2O–$Cu(OH)_2$ nanoparticles as a supercapacitor electrode material. They attained a specific capacitance 425 F g^{-1} in 0.5 M Na_2SO_4 electrolyte. Li et al. [37] synthesized CuO thin films and its different nanostructures using thermal method. He reported a

* Corresponding author.
E-mail address: sbpkim@dongguk.edu (D.Y. Kim).

https://doi.org/10.1016/j.colsurfb.2019.05.079
Received 22 January 2019; Received in revised form 20 May 2019; Accepted 22 May 2019
Available online 27 June 2019

specific capacitance of 212 F g^{-1} in a KOH electrolyte for CuO thin films. However, the literature contains few reports on the use of Cu_2O in supercapacitor electrodes. Patake et al. [38] produced Cu_2O thin films by electrodeposition for supercapacitors application and attained a specific capacitance of 36 F g^{-1}. Dong et al. [39] prepared Cu_2O thin films on copper foil for supercapacitor applications, resulting in an electrode with a maximum specific capacitance of 862 F g^{-1} after 20 cycles. Hence, copper oxide thin films with different morphologies have been used as supercapacitor electrodes, and the effects of the different nanostructures on their supercapacitive performance have been reported.

In this paper, we report on an important aspect of supercapacitor applications, wherein nanostructure morphology is improved using different ionic liquids. In particular, the effects of the ionic liquids 2-dimethylimidazolium chloride [HPDMIM(C1)], 1-(2′,3′-dihydroxypropyl)-3-methylimidazolium chloride [DHPMIM(C1)], *N*-(3-methyl-2-oxopropyl)pyridine chloride [MOCPP(C1)] on the morphological evolution and pseudocapacitive performance CuO thin-film supercapacitor electrodes synthesized through a chemical bath deposition (CBD) method is studied. The effect of the ionic liquids on the physiochemical properties of these CuO nanosheets films was investigated through various analysis techniques such as X-ray diffraction (XRD), X-ray photoelectron spectroscopy (XPS), scanning electron microscopy (SEM), and Fourier transform infrared (FT-IR) spectroscopy. The supercapacitive properties of CuO nanosheet electrodes functionalized with [HPDMIM(C1)], [DHPMIM(C1)], and [MOCPP(C1)] were investigated through cyclic voltammetry (CV), galvanostatic charge–-discharge, and electrochemical impedance spectroscopy (EIS) techniques.

2. Experimental details

2.1. Materials

Copper(II) sulfate ($CuSO_4$), sodium sulfate (Na_2SO_4), ammonia (NH_3), $5H_2O$, 2-dimethylimidazolium chloride [HPDMIM(C1)], 1-(2′,3′-dihydroxypropyl)-3-methylimidazolium chloride [DHPMIM(C1)], N-(3-methyl-2-oxopropyl)pyridine chloride [MOCPP(C1)] were purchased from SD-Fine Chem.

2.2. Preparation of CuO

Pure CuO, HPDMIM(C1):CuO, DHPMIM(C1):CuO, and MOCPP (C1):CuO thin films were deposited through CBD. Briefly, a 100 mL aqueous solution of 0.1 M $CuSO_4$ was used as the copper source and aqueous ammonia was used as a complexing agent [40–42]. The final concentration of the ionic liquids was 0.1 mM for HPDMIM(C1), DHPMIM(C1), and MOCPP(C1). The resulting pH of the solutions was ˜11 after 3.5 mL of ammonia was added. Prepared conducting stainless steel (SS) substrate was immersed in the solutions, and the bath was then heated to 342 K to initiate precipitation. Upon precipitation, the heterogeneous reaction on the SS substrate led to deposition of copper oxide after 40 min [43]. The stainless steel substrate treated with CuO films was washed with double-distilled water, air-dried, and used for further analysis.

2.3. Characterization

Structural analyses of pure CuO, HPDMIM(C1):CuO, DHPMIM (C1):CuO, and MOCPP(C1):CuO samples were performed using a Philips PW-3710 X-ray diffractometer equipped with a Cu K_α radiation source (λ = 1.54 Å). XPS was carried out using a VG Multilab 2000 (Thermo VG Scientific, UK), and the film surface morphology was observed by field-emission scanning electron microscopy (FE-SEM, Nova NanoSEM 200).

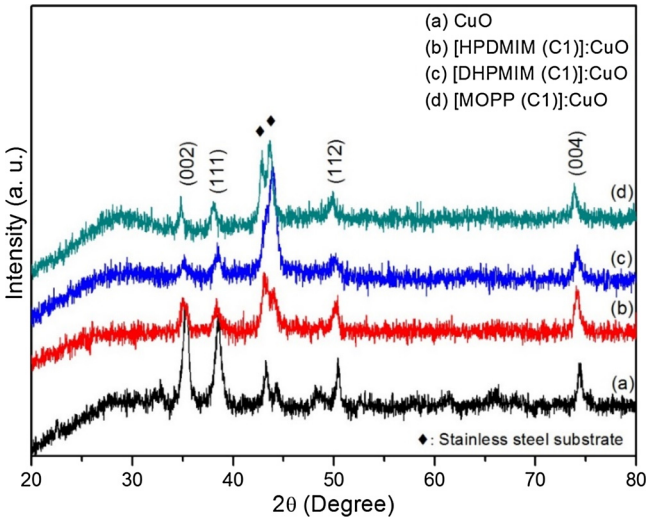

Fig. 1. XRD patterns of the (a) pure, ionic liquid functionalized with (b) HPDMIM (C1), (c) DHPMIM (C1), (d) MOCPP (C1) with CuO thin films synthesized by chemical bath deposition method, respectively.

2.4. Electrolyte preparation for electrochemical measurements

To examine the supercapacitor performance, CV and galvanostatic charge–discharge measurements were conducted using a CH Instruments CHI-600D electrochemical workstation with a conventional three-electrode system. We used as-prepared CuO, HPDMIM (C1):CuO, DHPMIM(C1):CuO, and MOCPP(C1):CuO as working electrodes with unit dimensions of 1 × 1 cm^2, platinum as a counter electrode, and a Ag/AgCl electrode as a reference electrode in a 1 M Na_2SO_4 aqueous electrolyte solution. EIS was carried out using a ZIVE SP5 electrochemical workstation.

3. Results and discussion

3.1. Crystal structure studies

XRD was used for the structural analysis and phase identification of the as-synthesized CuO thin films. Fig. 1(a–d) displays the XRD patterns of the pure CuO thin film and the CuO samples functionalized with different ionic liquids. The XRD patterns show no impurity peaks, confirming the phase purity of the samples. The observed peak positions were matched to those of the pure monoclinic phase of CuO (JCPDS card No. 48-1548); specifically, the diffraction peaks at 34.89°, 38.15°, 49.90°, and 73.90° were indexed to the (002), (111), (112), and (004) planes, respectively [44,45]. The phase purity of all of the samples confirmed that the ionic liquids are useful for modifying the microstructure of the CuO thin films. The crystallite size (*D*) of all the CuO samples was calculated from their respective XRD patterns using the Scherrer relation (1):

$$D = \frac{0.9\lambda}{\beta\cos\theta} \quad (1)$$

where β is the full-width at half-maximum (FWHM) and $\lambda = 1.54056$ Å, the wavelength of the Cu K_α-rays. The D values of the different CuO thin films are shown in Table 1. The results indicate that, compared with the D values in the pure CuO films that in the CuO films functionalized with an ionic liquid decreased. Therefore, the treatment with ionic liquid increased the specific surface area of the films. On the basis of the XRD results, we concluded that the ionic liquids did not disturb the structural properties of the CuO thin films [43,45].

Table 1
Crystallite size and EIS parameters of pure CuO thin films and functionalized with different ionic liquids like HPDMIM (C1), DHPMIM (C1), MOCPP(C1).

Electrodes	Crystallite size D (nm)	Solution resistance (R_S) Ω	Charge transfer resistance (R_{ct}) Ω
Pure CuO	85	2.6	11
HPDMIM (C1):CuO	41	1.40	2.4
DHPMIM (C1):CuO	42	1.56	6.55
MOPP (C1):CuO	50	2.0	8.48

3.2. X-ray photoelectron spectroscopy analysis studies

The elemental composition of the chemically deposited CuO was further confirmed using XPS analysis to identify the oxidation and elemental states of copper and oxygen. Fig. 2a shows the survey spectrum of the CuO functionalized with the optimized ionic liquid HPDMIM(C1). The survey spectrum confirms the presence of copper, carbon, and oxygen elements. Fig. 2(b–d) shows the high-resolution Cu 2p, O 1s, and C 1s spectra, respectively. The Cu 2p high-resolution spectrum indicates the two peaks observed at 933.55 and 953.59 eV, which related to Cu $2p_{3/2}$ and Cu $2p_{1/2}$, respectively. Similar observations have been previously reported [43]. Fig. 2c shows the O 1s high-resolution spectra of the CuO samples, which include a peak at a binding energy of 529.56 eV, which indicates formation of CuO thin films [46–48]. Fig. 2d displays the high-resolution C 1s spectrum, with a peak at a binding energy at 284.53 eV. Thus, the results of the XRD and XPS analyses confirm the formation of CuO thin films without any inorganic impurities.

3.3. Fourier transform infrared spectroscopy studies

Fig. 3(a, b) shows the FT-IR spectra of the CuO thin film and the films functionalized with the optimized HPDMIM(C1) ionic liquid, respectively. The characteristics peaks are appeared at 511, 599, and 688 cm^{-1}. These peaks correspond to the CuO vibrations of the monoclinic phase, indicating the formation of CuO [49]. Also, the absorption peak at 729 cm^{-1} is related to Cu—O stretching modes [50,51]. In Fig. 3(a, b), similar vibration bands are observed at 876 and 1369 cm^{-1}, which correspond to the C—C and C—O stretching vibration modes, respectively [52]. Therefore, the FT-IR studies further supported the XRD results by confirming the formation of pure CuO samples.

3.4. Scanning electron microscopy studies

Fig. 4(a–h) shows SEM micrographs of the chemically deposited ionic liquids and pure CuO nanostructures at two different magnifications. Substantial information regarding the surface morphology of the pure CuO samples was obtained from the micrographs, wherein nanosheets-like and hybrid nanostructures appeared after the functionalization with ionic liquids. Fig. 4(a, b) shows the foundation of the well-arranged hierarchical nanosheets that appeared to be homogeneously deposited over the steel substrate. These small interconnected sheets create abundant space, suggesting easy electrolyte ion transport and more superficial electroactive species [53]. In the case of CuO

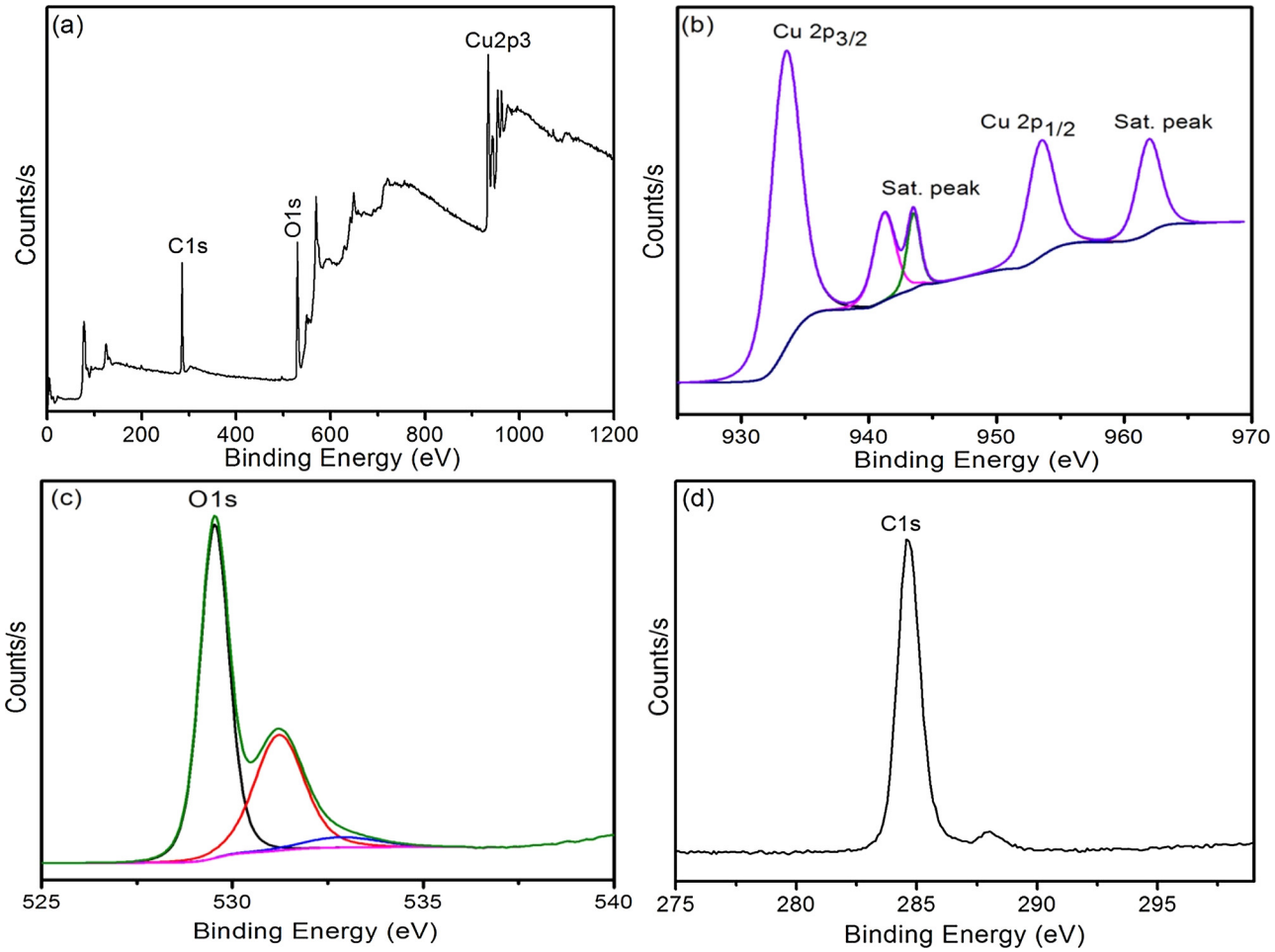

Fig. 2. (a) XPS survey spectrum, (b) high-resolution spectrum of Cu 2p, (c) high-resolution specrum of O1 s, and high-resolution spectrum of C1 s, HPDMIM (C1) functionalized with CuO thin films, respectively.

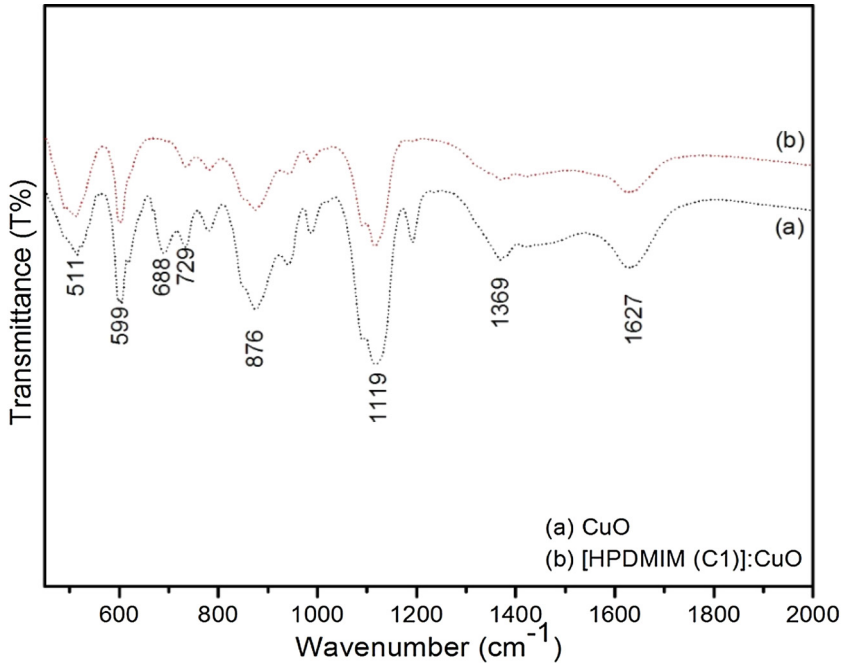

Fig. 3. (a) FT-IR spectrum of the pure, and (b) HPDMIM (C1) functionalized with CuO thin films synthesized by chemical bath deposition method, respectively.

functionalized with the ionic liquid HPDMIM(C1), its morphology substantially changed from nanosheets to hybrid nanostructures in which nanowires were interconnected with each other to form a nanoflake-like network (Fig. 4(c, d)); such a morphology should enhance charge transport at the electrolyte–electrode interface. When the ionic liquid DHPMIM(C1) was used to modify CuO, spherical nanoflake-like CuO composed of large numbers of tiny flakes was formed (Fig. 4(e, f)). This morphology offers a more reactive surface and is beneficial to ion transport [54]. In addition, it produces a porous surface and crevices that result in a large reactive surface for faster diffusion of electrolyte when used in supercapacitor applications. No considerable difference was observed in the morphology of the MOCPP(C1):CuO (Fig. 4(g, h)). In summary, the treatment of CuO with ionic liquids considerably changed the surface properties of the CuO thin films [55–58].

3.5. Electrochemical impedance spectroscopy studies

We conducted EIS to investigate the relationship between the interfacial electronic properties of the Na_2SO_4 electrolyte and the HPDMIM(C1):CuO, DHPMIM(C1):CuO, and MOCPP(C1):CuO electrodes. The Nyquist plots show capacitive performance impedance spectra for both CuO and the ionic-liquid-functionalized CuO electrodes (Fig. 5). The inset shows the equivalent circuit, and Table 1 shows the values of the solution resistance (R_s) and the charge transfer resistance (R_{ct}). Notably, the HPDMIM(C1):CuO sample exhibited lower R_s values, displaying better conduction in the electrolyte and a low internal resistance of the capacitor (Table 1). The R_{ct} value for the HPDMIM (C1):CuO electrode is also low compared with those for the other electrodes, indicating better ionic conduction and greater electrolyte diffusion to the CuO nanosheets [59–61]. For the pure CuO, HPDMIM (C1):CuO, DHPMIM(C1):CuO, and MOCPP(C1):CuO electrodes, the R_s values are approximately 2.6, 1.40, 1.56, and 2.0 Ω, respectively. In addition, the R_{ct} value for the pure CuO electrode (11 Ω) decreased after functionalization with the ionic liquids (Table 1). For the HPDMIM(C1):CuO, DHPMIM(C1):CuO, and MOCPP(C1):CuO electrodes, the R_{ct} values are 2.4, 6.55 and 8.49 Ω, respectively. These results demonstrate that the solution resistance and series resistance [55] are lowest for the ionic-liquid-functionalized electrodes, suggesting that the CuO electrodes offer greater interfacial area after functionalization with the ionic liquids. All of these results are useful for increasing the value of the specific capacitance related to the pure CuO electrodes. They also suggest that the HPDMIM(C1):CuO electrode should exhibit better performance in supercapacitor applications. In summary, we conclude that the HPDMIM(C1)-functionalized CuO electrode exhibits better capacitive behavior than the pure CuO, DHPMIM(C1):CuO, and MOCPP(C1):CuO electrodes.

3.6. Cyclic voltammetry studies

Fig. 6(a, b) shows the CV curves and specific capacitance of different ionic-liquid-functionalized CuO electrodes at a scan rate of 100 mV s^{-1} in 1 M Na_2SO_4 aqueous electrolyte, respectively. The specific capacitance (C_s) measurements and CV curves indicate that ionic-liquid functionalization resulted in CuO nanosheets with enhanced specific capacitance. These observations are connected to the surface morphological alterations as well as porosity of the CuO thin films due to the different ionic-liquids. After functionalization with the HPDMIM(C1) ionic liquid, the CuO film exhibited a change in surface morphology from nanosheets to a hybrid nanostructure composed of nanobuds and 3D-blades that, compared with other pure CuO nanostructures, should offer additional electroactive sites, thereby increasing the current density in a supercapacitor. The C_s of the CuO electrode was calculated by the standard relation [62]:

$$C_s = \frac{1}{mv(V_c - V_a)} \int_{V_a}^{V_c} I(V)dV \quad (2)$$

where C_s is the specific capacitance (F g^{-1}), v is the potential scan rate (mV s^{-1}), ($V_c - V_a$) is the potential window (0 to +0.9 V), I is the response current (mA), and m is the deposited weight of the electrode. The maximum values of the C_s were found to be 60 F g^{-1} for the CuO, 198 F g^{-1} for HPDMIM(C1), 144 F g^{-1} for DHPMIM(C1), and 80 F g^{-1} for MOCPP(C1) at a scan rate of 100 mV s^{-1} (Fig. 6b). The highest C_s for the HPDMIM(C1):CuO electrode is attributable to its hybrid surface morphology, where the addition of the ionic liquid increased the ionic conductivity of the CuO electrode. Although the literature contains numerous reports on the supercapacitor performance of CuO thin films, none have focused on the effects of different ionic liquids on their supercapacitive behavior. For instance, Shinde et al. [55] synthesized

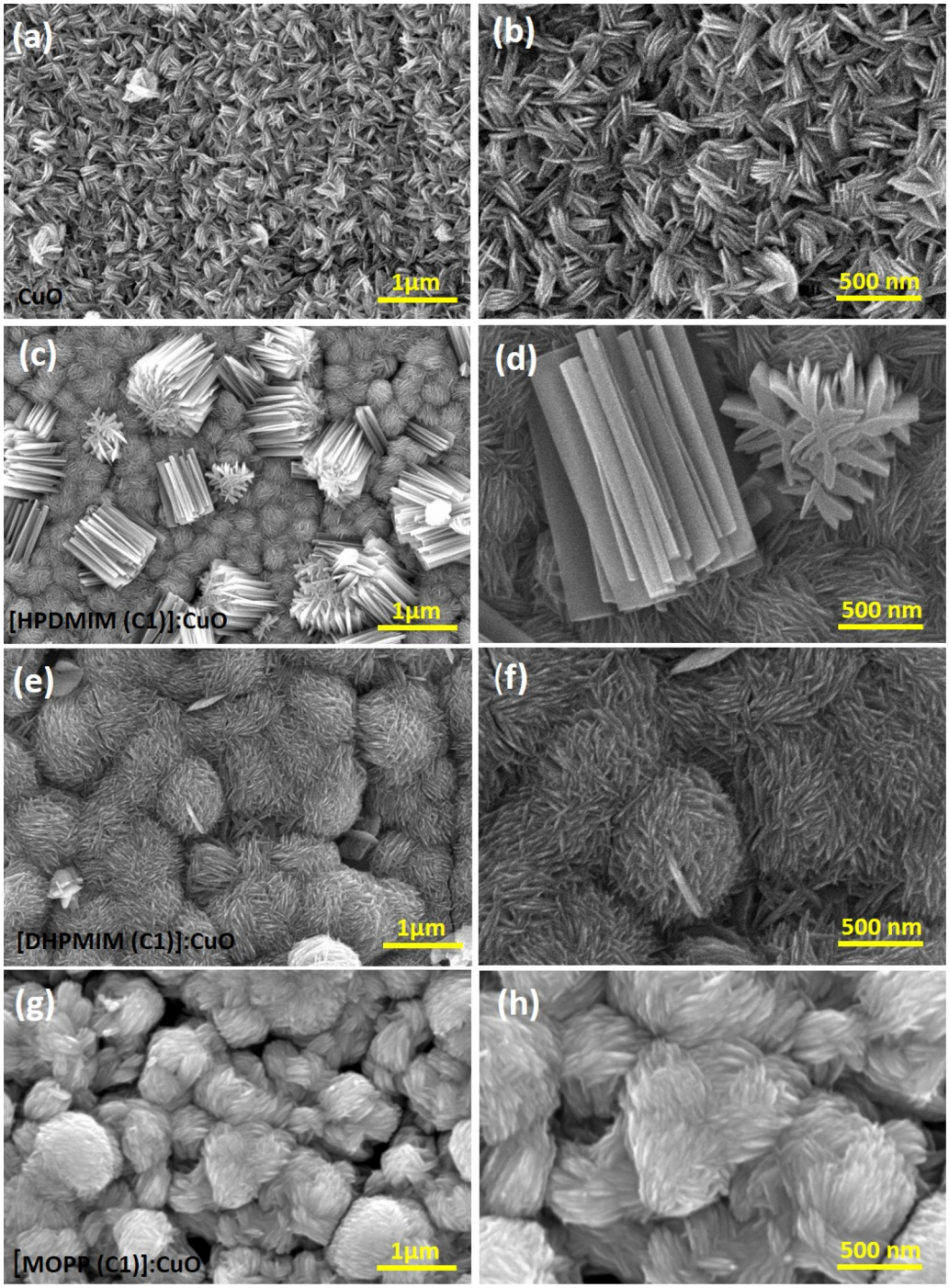

Fig. 4. SEM images of the (a) pure, and ionic liquid functionalized with (b) HPDMIM (C1), (c) DHPMIM (C1), (d) MOCPP (C1) with CuO thin films with different magnifications, respectively.

Mn:CuO/$Cu(OH)_2$ thin films through a SILAR method and they reported 3% Mn doping shows the highest specific capacitance (600 F g^{-1}). Navathe et al. [61] deposited CuO thin film via a hydrothermal technique using different percentages of a 3-(10-hydroxypropyl)-1-methylimidazolium chloride [HPMIM(Cl)] ionic liquid with a specific capacitance of 60 F g^{-1}. The enhancement in the specific capacitance of nanobuds such as CuO hybrids are mostly attributable to the effective utilization of the CuO because of the formation of hybrid nanostructures.

Fig. 6c presents the CV curves of HPDMIM(C1)-functionalized CuO at different scan rates (5–100 mV s^{-1}). Fig. 6d shows that the specific capacitance decreases with increasing scan rate and that the HPDMIM (C1) was a better ionic liquid for functionalizing the CuO to improvement in supercapacitor performance [55,61]. The outstanding specific capacitance value observed for the [HPDMIM(C1)]:CuO electrode is attributed to its structural network and more abundant conductive sites that led to the formation of the hybrid nanobud-like structures, which in turn enabled fast charge transport during reaction between the electrode and electrolyte.

3.7. Galvanostatic charge–discharge studies

To investigate rate capability, we evaluated the GCD performance of the CuO functionalized with the HPDMIM(C1) ionic liquid at different

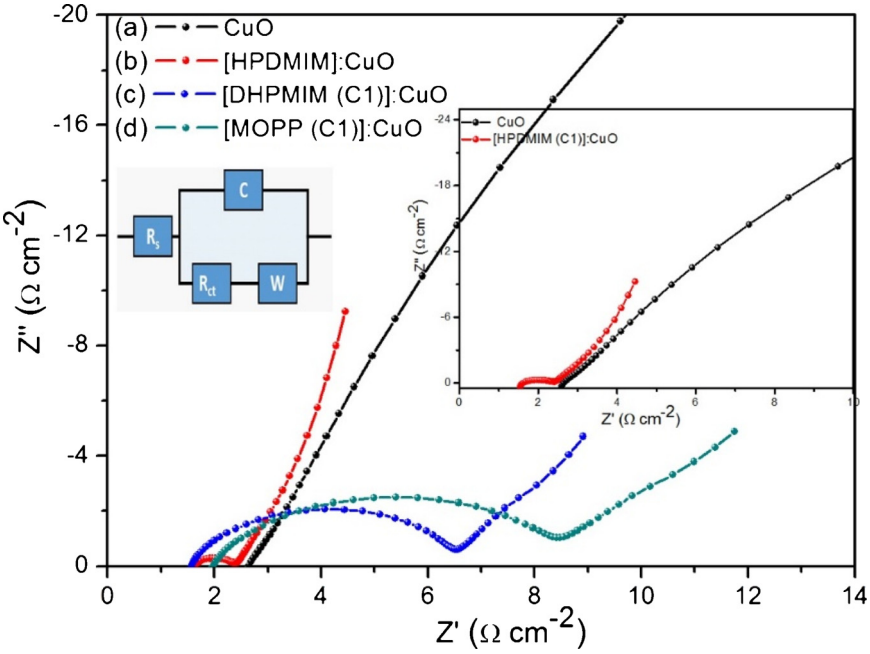

Fig. 5. Nyquist plots of the (a) pure, and ionic liquid functionalized with (b) HPDMIM (C1), (c) DHPMIM (C1), (d) MOCPP (C1) with CuO thin films, and inset show the equivalent circuit as well as high magnified images of pure CuO and optimized sample, respectively.

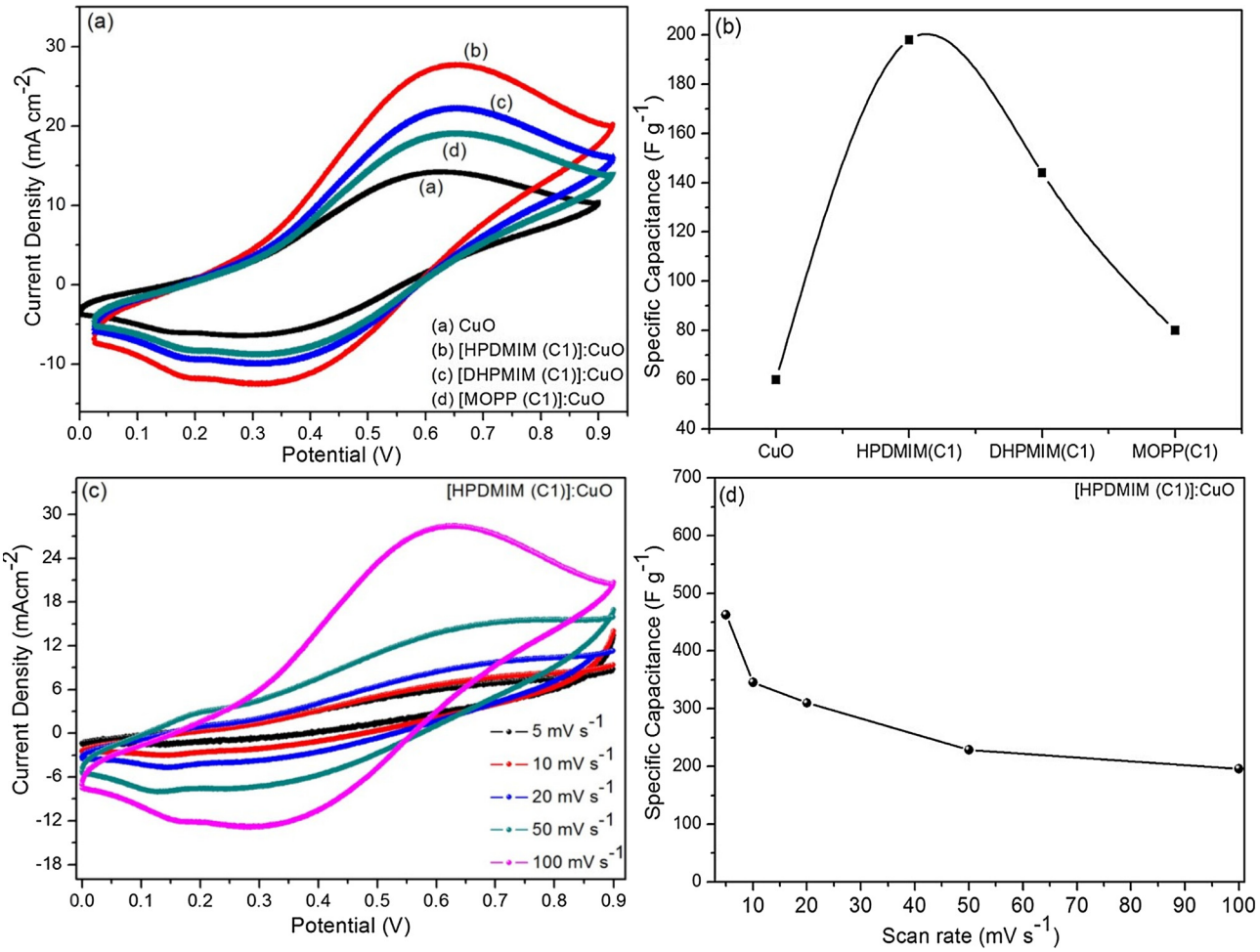

Fig. 6. (a) CV curves of the (a) pure, and ionic liquid functionalized with (b) HPDMIM (C1), (c) DHPMIM (C1), (d) MOCPP (C1) with CuO thin films at 100 mV s^{-1} with potential window 0 to 0.9 V, respectively, (b) Specific capacitance of the pure CuO and functionalized with different ionic liquids at 100 mV s^{-1} scan rate, respectively, (c) CV curves of the HPDMIM (C1) functionalized with CuO thin film at different scan rate from 5–100 mV s^{-1} with potential window 0–0.9 V, respectively (d) Specific capacitance of the optimized ionic liquid HPDMIM (C1) functionalized CuO with respect to the different scan rate.

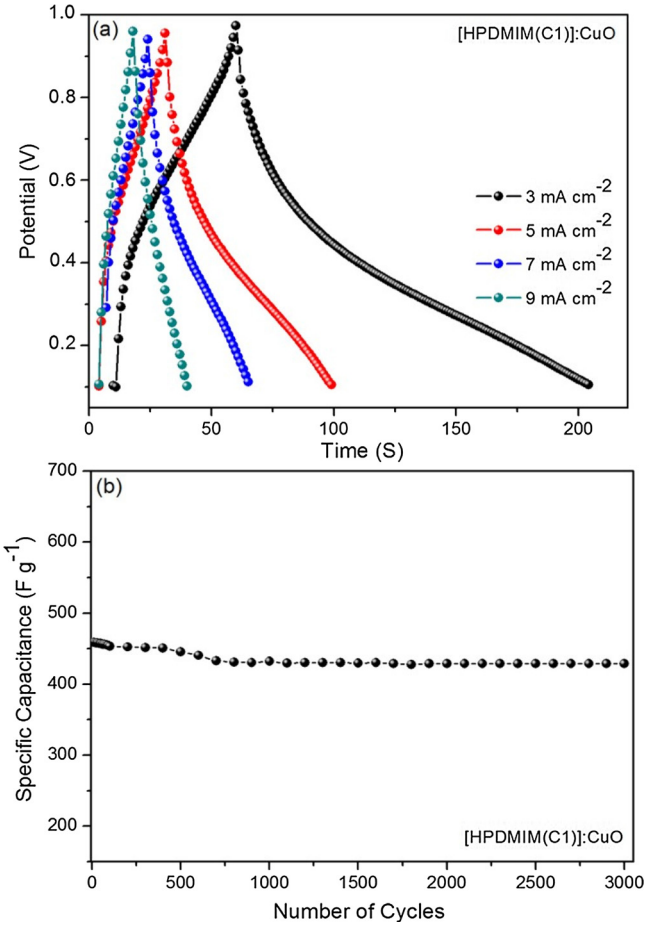

Fig. 7. (a) Galvanostatic charge–discharge, and (b) Cyclic stability of optimized ionic liquid HPDMIM (C1):CuO electrodes at 100 mV s^{-1} scan rate up to 3000 cycles.

current densities (Fig. 7a). The charge and discharge curves shows the charge and discharge shapes were approximately equal, confirming the material's pseudocapacitive behavior. Notably, the discharge curves for the CuO electrodes functionalized with HPDMIM(C1) revealed the "iR" drop is very low, indicating good electrical conductivity of the electrode material. This behavior may be due to the incorporation of the HPDMIM(C1) ionic liquid into CuO as well as the resulting unique nanostructure [63]. Fig. 7b represents the specific capacitance of the HPDMIM(C1)-functionalized CuO thin films with respect to the number cycles at a scan rate of 5 mV s^{-1}. The entire CuO electrode exhibited good cycling stability of approximately 89% specific capacitance retention after 3000 cycles. A potential explanation for this cycling stability is the unique nanostructure and greater electronic conductivity of the HPDMIM(C1):CuO electrode, which sustains the volume expansion of the material during charge/discharge cycling [60–64].

4. Conclusion

In conclusion, we have successfully examined the effects of different ionic liquids on the structural, morphological and supercapacitive properties of nanosheet-like CuO hybrid electrodes synthesized through CBD. Our obtained results shown the development of CuO electrodes with substantial morphological variation. Furthermore, we observed that the ionic liquid expressively changed the supercapacitor performance of the CuO electrodes. The results showed that the HPDMIM (C1):CuO electrodes with nanobud-like hybrid nanostructures exhibited a high specific capacitance of 464 F g^{-1} at a scan rate of 5 mV s^{-1}. The main approach proposed in the present work is easy and simple, where the ionic liquid used for functionalization affects the electrochemical performance and surface morphology of CuO films.

Acknowledgment

This work was supported by the Dongguk University Research Fund of 2018.

References

[1] J. Cherusseri, K.K. Kar, Hierarchically mesoporous carbon nanopetal based electrodes for flexible supercapacitors with super-long cyclic stability, J. Mater. Chem. A Mater. Energy Sustain. 3 (2015) 21586–21598.
[2] L. Sun, C. Tian, M. Li, X. Meng, L. Wang, R. Wang, J. Yin, H. Fu, From coconut shell to porous graphene-like nanosheets for high-power supercapacitors, J. Mater. Chem. A Mater. Energy Sustain. 1 (2013) 6462–6470.
[3] M.M. Shaijumon, F.S. Ou, L. Ci, P.M. Ajayan, Synthesis of hybrid nanowire arrays and their application as high power supercapacitor electrodes, Chem. Commun. (Camb.) 2374 (2008) 2373–2375.
[4] X. Fan, H. Zhou, X. Guo, Growth of carbon composites by grafting on pregrown vertically aligned single-walled carbon nanotube arrays and their use in high power supercapacitors, RSC Adv. 5 (2015) 45484–45491.
[5] C.G. Morales-Guio, S.D. Tilley, H. Vrubel, M. Grätzel, X. Hu, Hydrogen evolution from a copper (I) oxide photocathode coated with an amorphous molybdenum sulphide catalyst, Nat. Commun. 5 (2014) 3059–3066.
[6] S. Gao, Y. Sun, F. Lei, J. Liu, L. Liang, T. Li, B. Pan, J. Zhou, Y. Xie, Freestanding atomically-thin cuprous oxide sheets for improved visible-light photoelectrochemical water splitting, Nano Energy 8 (2014) 205–213.
[7] L. Zhu, M. Hong, G.W. Ho, Fabrication of wheat grain textured TiO_2/CuO composite nanofibers for enhanced solar H_2 generation and degradation performance, Nano Energy 11 (2015) 28–37.
[8] J. Azevedo, L. Steier, P. Dias, M. Stefik, C.T. Sousa, J.P. Araújo, A. Mendes, M. Graetzel, S.D. Tilley, On the stability enhancement of cuprous oxide water splitting photocathodes by low temperature steam annealing, Energy Environ. Sci. 7 (2014) 4044–4052.
[9] A. Paracchino, V. Laporte, K. Sivula, M. Grätzel, E. Thimsen, Highly active oxide photocathode for photoelectrochemical water reduction, Nat. Mater. 10 (2011) 456–461.
[10] P. Rai, R. Khan, S. Raj, S.M. Majhi, K.-K. Park, Y.-T. Yu, I.-H. Lee, P.K. Sekhar, Au@Cu_2O core–shell nanoparticles as chemiresistors for gas sensor applications: effect of potential barrier modulation on the sensing performance, Nanoscale 6 (2014) 581–588.
[11] Y.S. Lee, D. Chua, R.E. Brandt, S.C. Siah, J.V. Li, J.P. Mailoa, S.W. Lee, R.G. Gordon, T. Buonassisi, Atomic layer deposited gallium oxide buffer layer enables 1.2 V open-circuit voltage in cuprous oxide solar cells, Adv. Mater. 26 (2014) 4704–4710.
[12] R.-C. Wang, P.-H. Huang, P.-C. Chuang, Y.-C. Li, Enhanced rate capability of pseudocapacitive CuO by incorporation of Li for excellent composite electrode, J. Electroanal. Chem. Lausanne (Lausanne) 39 (2019) 160–165.
[13] S. Masudy-Panah, K. Radhakrishnan, H.R. Tan, R. Yi, T.I. Wong, G.K. Dalapati, Titanium doped cupric oxide for photovoltaic application, Sol. Energy Mater. Sol. Cells 140 (2015) 266–274.
[14] S. Masudy-Panah, G.K. Dalapati, K. Radhakrishnan, A. Kumar, H.R. Tan, Reduction of Cu-rich interfacial layer and improvement of bulk CuO property through two-step sputtering for p-CuO/n-Si heterojunction solar cell, J. Appl. Phys. 116 (2014) 074501-074501.
[15] S. Masudy-Panah, R. Siavash Moakhar, C.S. Chua, H.R. Tan, T.I. Wong, D. Chi, G.K. Dalapati, Nanocrystal engineering of sputter-grown CuO photocathode for visible-light-driven electrochemical water splitting, ACS Appl. Mater. Interfaces 8 (2016) 1206–1213.
[16] G. Fan, F. Li, Effect of sodium borohydride on growth process of controlled flower-like nanostructured Cu_2O/CuO films and their hydrophobic property, Chem. Eng. J. 167 (2011) 388–396.
[17] H. Li, S. Yu, X. Han, Fabrication of CuO hierarchical flower-like structures with biomimetic superamphiphobic, self-cleaning and corrosion resistance properties, Chem. Eng. J. 283 (2016) 1443–1454.
[18] Y. Ma, H. Li, R. Wang, H. Wang, W. Lv, S. Ji, Ultrathin willow-like CuO nanoflakes as an efficient catalyst for electro-oxidation of hydrazine, J. Power Sources 289 (2015) 22–25.
[19] Y. Ma, H. Wang, J. Key, S. Ji, W. Lv, R. Wang, Control of CuO nanocrystal morphology from ultrathin "willow-leaf" to "flower-shaped" for increased hydrazine oxidation activity, J. Power Sources 300 (2015) 344–350.
[20] D.P. Dubal, G.S. Gund, R. Holze, C.D. Lokhande, Mild chemical strategy to grow micro-roses and micro-woolen like arranged CuO nanosheets for high performance supercapacitors, J. Power Sources 242 (2013) 687–698.
[21] G. Wang, J. Huang, S. Chen, Y. Gao, D. Cao, Preparation and supercapacitance of CuO nanosheet arrays grown on nickel foam, J. Power Sources 196 (2011) 5756–5760.
[22] A.C. Nwanya, D. Obi, K.I. Ozoemena, R.U. Osuji, C. Awada, A. Ruediger, M. Maaza, F. Rosei, F.I. Ezema, Facile synthesis of nanosheet-like CuO film and its potential application as a high-performance pseudocapacitor electrode, Electrochim. Acta 198 (2016) 220–230.
[23] W. Zhang, H. Wang, Y. Zhang, Z. Yang, Q. Wang, J. Xia, X. Yang, Facile micro-emulsion synthesis of porous CuO nanosphere film and its application in lithium ion

batteries, Electrochim. Acta 113 (2013) 63–68.
[24] J. Wang, W.-D. Zhang, Fabrication of CuO nanoplatelets for highly sensitive enzyme-free determination of glucose, Electrochim. Acta 56 (2011) 7510–7516.
[25] F. Cao, X.H. Xia, G.X. Pan, J. Chen, Y.J. Zhang, Construction of carbon nanoflakes shell on CuO nanowires core as enhanced core/shell arrays anode of lithium ion batteries, Electrochim. Acta 178 (2015) 574–579.
[26] B. Heng, C. Qing, D. Sun, B. Wang, H. Wang, Y. Tang, Rapid synthesis of CuO nanoribbons and nanoflowers from the same reaction system, and a comparison of their supercapacitor performance, RSC Adv. 3 (2013) 15719–15726.
[27] Z. Zhang, H. Che, Y. Wang, L. Song, Z. Zhong, F. Su, Preparation of hierarchical dandelion-like CuO microspheres with enhanced catalytic performance for dimethyldichlorosilane synthesis, Catal. Sci. Technol. 2 (2012) 1953–1960.
[28] M.-J. Deng, C.-C. Wang, P.-J. Ho, C.-M. Lin, J.-M. Chen, K.-T. Lu, Facile electrochemical synthesis of 3D nano-architectured CuO electrodes for high-performance supercapacitors, J. Mater. Chem. A Mater. Energy Sustain. 2 (2014) 12857–12865.
[29] S.E. Moosavifard, M.F. El-Kady, M.S. Rahmanifar, R.B. Kaner, M.F. Mousavi, Designing 3D highly ordered nanoporous CuO electrodes for high-performance asymmetric supercapacitors, ACS Appl. Mater. Interfaces 7 (2015) 4851–4860.
[30] W. Xu, S. Dai, G. Liu, Y. Xi, C. Hu, X. Wang, CuO Nanoflowers growing on carbon fiber fabric for flexible high-performance supercapacitors, Electrochim. Acta 203 (2016) 1–8.
[31] S.K. Shinde, M.B. Jalak, G.S. Ghodake, N.C. Maile, V.S. Kumbhar, D.S. Lee, V.J. Fulari, D.-Y. Kim, Chemically synthesized nanoflakes-like $NiCo_2S_4$ electrodes for high-performance supercapacitor application, Appl. Surf. Sci. 466 (2019) 822–829.
[32] D.P. Dubal, G.S. Gund, R. Holze, H.S. Jadhav, C.D. Lokhande, C.-J. Park, Surfactant-assisted morphological tuning of hierarchical CuO thin films for electrochemical supercapacitors, Dalton Trans. 42 (2013) 6459–6467.
[33] S.K. Shinde, D.P. Dubal, G.S. Ghodake, V.J. Fulari, Hierarchical 3D-flower-like CuO nanostructure on copper foil for supercapacitors, RSC Adv. 5 (2015) 4443–4447.
[34] S.K. Shinde, D.P. Dubal, G.S. Ghodake, D.Y. Kim, V.J. Fulari, Nanoflower-like CuO/$Cu(OH)_2$ hybrid thin films: synthesis and electrochemical supercapacitive properties, J. Electroanal. Chem. Lausanne (Lausanne) 732 (2014) 80–85.
[35] J. Zhang, H. Feng, Q. Qin, G. Zhang, Y. Cui, Z. Chai, W. Zheng, Interior design of three-dimensional CuO ordered architectures with enhanced performance for supercapacitors, J. Mater. Chem. A Mater. Energy Sustain. 4 (2016) 6357–6367.
[36] S. Ghasemi, M. Jafari, F. Ahmadi, Cu_2O-$Cu(OH)_2$-graphene nanohybrid as new capacitive material for high performance supercapacitor, Electrochim. Acta 210 (2016) 225–235.
[37] Y. Li, S. Chang, X. Liu, J. Huang, J. Yin, G. Wang, D. Cao, Nanostructured CuO directly grown on copper foam and their supercapacitance performance, Electrochim. Acta 85 (2012) 393–398.
[38] V.D. Patake, S.S. Joshi, C.D. Lokhande, O.-S. Joo, Electrodeposited porous and amorphous copper oxide film for application in supercapacitor, Mater. Chem. Phys. 114 (2009) 6–9, https://doi.org/10.1016/j.matchemphys.2008.09.031.
[39] C. Dong, Y. Wang, J. Xu, G. Cheng, W. Yang, T. Kou, Z. Zhang, Y. Ding, 3D binder-free Cu2O@Cu nanoneedle arrays for high-performance asymmetric supercapacitors, J. Mater. Chem. A Mater. Energy Sustain. 2 (2014) 18229–18235.
[40] S. Shinde, H. Dhaygude, D.-Y. Kim, G. Ghodake, P. Bhagwat, P. Dandge, V. Fulari, Improved synthesis of copper oxide nanosheets and its application in development of supercapacitor and antimicrobial agents, J. Ind. Eng. Chem. 36 (2016) 116–120.
[41] D.P. Dubal, D.S. Dhawale, R.R. Salunkhe, V.S. Jamdade, C.D. Lokhande, Fabrication of copper oxide multilayer nanosheets for supercapacitor application, J. Alloys. Compd. 492 (2010) 26–30.
[42] V. Senthilkumar, Y.S. Kim, S. Chandrasekaran, B. Rajagopalan, E.J. Kim, J.S. Chung, Comparative supercapacitance performance of CuO nanostructures for energy storage device applications, RSC Adv. 5 (2015) 20545–20553.
[43] M.F. Al-Kuhaili, Characterization of copper oxide thin films deposited by the thermal evaporation of cuprous oxide (Cu_2O), Vacuum 82 (2008) 623–629.
[44] N. Mukherjee, B. Show, S.K. Maji, U. Madhu, S.K. Bhar, B.C. Mitra, G.G. Khan, A. Mondal, CuO nano-whiskers: electrodeposition, Raman analysis, photoluminescence study and photocatalytic activity, Mater. Lett. 65 (2011) 3248–3250.
[45] A. Mahmood, F. Tezcan, G. Kardas, Photoelectrochemical characteristics of CuO films with different electrodeposition time, Int. J. Hydrogen Energ. 42 (2017) 23268–23275.
[46] A. Tadjarodi, O. Akhavan, K. Bijanzad, Photocatalytic activity of CuO nanoparticles incorporated in mesoporous structure prepared from bis(2-aminonicotinato) copper (II) microflakes, Trans. Nonferrous Met. Soc. China 25 (2015) 3634–3642.
[47] L.-J. Chen, G.-S. Li, L.-P. Li, CuO nanocrystals in thermal decomposition of ammonium perchlorate, J. Therm. Anal. Calorim. 91 (2008) 581–587.
[48] S.K. Shinde, D.-Y. Kim, G.S. Ghodake, N.C. Maile, A.A. Kadam, D.S. Lee, M.C. Rath, V.J. Fulari, Morphological enhancement to CuO nanostructures by electron beam irradiation for biocompatibility and electrochemical performance, Ultrason Sonochemistry. 40 (2018) 314–322.
[49] S.K. Shinde, G.S. Ghodake, V.J. Fulari, D.-Y. Kim, High electrochemical performance of nanoflakes like CuO electrode by successive ionic layer adsorption and reaction (SILAR) method, J. Ind. Eng. Chem. 52 (2017) 12–17.
[50] H. Cavusoglu, R. Aydin, Complexing agent triethanolamine mediated synthesis of nanocrystalline CuO thin films at room temperature via SILAR technique, Superlattice. Microst. 128 (2019) 37–47.
[51] B. Talluri, E. Prasad, T. Thomas, Critical role of surfactants in the formation of digestively-ripened, ultra-small (r < 2 nm) copper oxide quantum dots, Superlattice. Microst. 116 (2018) 122–130.
[52] M. Vaseem, A. Umar, S.H. Kim, Y.B. Hahn, Low-Temperature synthesis of flower-shaped CuO nanostructures by solution process: Formation mechanism and structural properties, J. Phys. Chem. C 112 (2008) 5729–5735.
[53] D. Saravanakkumar, H.A. Oualid, Y. Brahmi, A. Ayeshamariam, M. Karunanaithy, A.M. Saleem, K. Kaviyarasu, S. Sivaranjani, M. Jayachandran, Synthesis and characterization of CuO/ZnO/CNTs thin films on copper substrate and its photocatalytic applications, Open Nano 4 (2019) 100025–100040.
[54] S.K. Shindea, M.B. Jalak, G.S. Ghodake, N.C. Maile, V.S. Kumbhar, D.S. Lee, V.J. Fulari, D.-Y. Kim, Chemically synthesized nanoflakes-like $NiCo_2S_4$ electrodes for high-performance supercapacitor application, Appl. Surf. Sci. 466 (2019) 822–829.
[55] S.K. Shinde, M.B. Jalak, S.Y. Kim, H.M. Yadav, G.S. Ghodake, A.A. Kadam, D.-Y. Kim, Effect of Mn doping on the chemical synthesis of interconnected nanoflakes-like CoS thin films for high performance supercapacitor applications, Ceram. Int. 44 (2018) 23102–23108.
[56] S.K. Shinde, D.P. Dubal, G.S. Ghodake, P. Gomez-Romero, S. Kim, V.J. Fulari, Influence of Mn incorporation on the supercapacitive properties of hybrid CuO/Cu$(OH)_2$ electrodes, RSC Adv. 5 (2015) 30478–30484.
[57] S.K. Shinde, D.P. Dubal, G.S. Ghodake, V.J. Fulari, Synthesis and characterization of chemically deposited flower-like $CdSe_{0.6}Te_{0.4}$ thin films for solar cell application, Mater. Lett. 126 (2014) 17–19.
[58] S.K. Shinde, G.S. Ghodake, D.P. Dubal, G.M. Lohar, D.S. Lee, V.J. Fulari, Structural, optical, and photo-electrochemical properties of marygold-like $CdSe_{0.6}Te_{0.4}$ synthesized by electrochemical route, Ceram. Int. 40 (2014) 11519–11524.
[59] Y. Gao, J. Zhao, Z. Run, G. Zhang, H. Pang, Microporous $Ni_{11}(HPO_3)_8(OH)_6$ nanocrystals for high-performance flexible asymmetric all solid-state supercapacitors, Dalton Trans. 43 (2014) 17000–17005.
[60] L. Mai, H. Li, Y. Zhao, L. Xu, X. Xu, Y. Luo, Z. Zhang, W. Ke, C. Niu, Q. Zhang, Fast ionic diffusion-enabled nanoflake electrode by spontaneous electrochemical pre-intercalation for high-performance supercapacitor, Sci. Rep. 3 (2013) 1718–1726.
[61] A.C. Nwanya, C. Awada, D. Obi, K. Raju, K.I. Ozoemena, R.U. Osuji, A. Ruediger, M. Maaza, F. Rosei, F.I. Ezema, Nanoporous copper-cobalt mixed oxide nanorod bundles as high performance pseudocapacitive electrodes, J. Electroanal. Chem. Lausanne (Lausanne) 787 (2017) 24–35.
[62] G.J. Navathe, D.S. Patil, P.R. Jadhav, D.V. Awale, A.M. Teli, S.C. Bhise, S.S. Kolekar, M.M. Karanjkar, J.H. Kim, P.S. Patil, Rapid synthesis of nanostructured copper oxide for electrochemical supercapacitor based on novel [HPMIM][Cl] ionic liquid, J. Electroanal. Chem. Lausanne (Lausanne) 738 (2015) 170–175.
[63] N.R. Chodankar, D.P. Dubal, G.S. Gund, C.D. Lokhande, Flexible all-solid-state MnO_2 thin films based symmetric supercapacitors, Electrochim. Acta 165 (2015) 338–347.
[64] J. Zhao, J. He, M. Sun, M. Qu, H. Pang, Nickel hydroxide–nickel nanohybrids indirectly from coordination microfibers for high-performance supercapacitor electrodes, Inorg. Chem. Front. 2 (2015) 129–135.